Bubble nucleation in simple and molecular liquids via the largest spherical cavity method

Miguel A. Gonzalez, José L. F. Abascal, Chantal Valeriani, and Fernando Bresme

Citation: The Journal of Chemical Physics **142**, 154903 (2015); doi: 10.1063/1.4916919
View online: http://dx.doi.org/10.1063/1.4916919
View Table of Contents: http://scitation.aip.org/content/aip/journal/jcp/142/15?ver=pdfcov
Published by the AIP Publishing

Bubble nucleation in simple and molecular liquids via the largest spherical cavity method

Miguel A. Gonzalez,[1,2,a)] José L. F. Abascal,[1] Chantal Valeriani,[1] and Fernando Bresme[2,3]
[1]*Departamento de Química Física, Facultad de Ciencias Químicas, Universidad Complutense de Madrid, 28040 Madrid, Spain*
[2]*Department of Chemistry, Imperial College London, London SW7 2AZ, United Kingdom*
[3]*Department of Chemistry, Norwegian University of Science and Technology, Trondheim, Norway*

(Received 8 January 2015; accepted 19 March 2015; published online 20 April 2015)

In this work, we propose a methodology to compute bubble nucleation free energy barriers using trajectories generated via molecular dynamics simulations. We follow the bubble nucleation process by means of a local order parameter, defined by the volume of the largest spherical cavity (LSC) formed in the nucleating trajectories. This order parameter simplifies considerably the monitoring of the nucleation events, as compared with the previous approaches which require *ad hoc* criteria to classify the atoms and molecules as liquid or vapor. The combination of the LSC and the mean first passage time technique can then be used to obtain the free energy curves. Upon computation of the cavity distribution function the nucleation rate and free-energy barrier can then be computed. We test our method against recent computations of bubble nucleation in simple liquids and water at negative pressures. We obtain free-energy barriers in good agreement with the previous works. The LSC method provides a versatile and computationally efficient route to estimate the volume of critical bubbles the nucleation rate and to compute bubble nucleation free-energies in both simple and molecular liquids. © *2015 AIP Publishing LLC.* [http://dx.doi.org/10.1063/1.4916919]

I. INTRODUCTION

The probability of forming the critical nucleus (crystal, droplet, or bubble) of a thermodynamically stable phase inside a thermodynamically metastable one is proportional to the nucleation free-energy barrier height. Classical Nucleation Theory[1] (CNT) provides a phenomenological approach to describe nucleation and to estimate the height of the free-energy barrier in terms of the interfacial tension between the two thermodynamically stable phases and the corresponding chemical potential difference. While CNT can provide reasonable values of the critical nucleus radius, it has been shown that it is not so accurate in predicting free-energy barrier heights and, as a consequence, nucleation rates, which can differ from the experimental ones by several orders of magnitude.[2–6] Statistical mechanics theories[4] and atomistic simulations[7–13] furnish a more detailed approach to study nucleation phenomena, allowing the calculation of free-energy barriers and nucleation rates, and offering microscopic insights into the nucleation mechanism. We exploit these techniques in this work to quantify bubble nucleation free-energy barriers in metastable liquids. Bubble nucleation is a phenomenon that is important in sonochemistry[14] and in the cavitation-induced surface erosion.[15]

The last decades have witnessed an increasing number of theoretical and computational studies devoted to vapour nucleation phenomena. Most of these works focused on simple superheated metastable liquids, such as Lennard-Jones (LJ). Shen and Debenedetti[10] used the umbrella sampling technique combined with a global order parameter, based on the total vapour density, to quantify the free-energy barrier and determine the size of the critical nucleus. They concluded that the shape of the critical nucleus corresponded to a system-spanning network, far from the spherical shape assumed by CNT. More recent works[11,16] have studied a superheated Lennard-Jones liquid similar to the one in Ref. 10, using the volume of the largest bubble as a local order parameter. It was found that the nucleation proceeds through the formation of spherical and compact critical bubbles, which agree with the description of the critical bubble being as an empty cavity.[6,17–24]

Bubble nucleation at negative pressures has received much less attention. Some of us have recently studied bubble nucleation in water at negative pressure.[22,25] In Ref. 22, the largest bubble volume was used as a local order parameter and the volume was estimated by a Voronoi polyhedra analysis. Very recently,[25] this problem has been revisited using two complementary methods inspired by Ref. 16. These approaches identified the volume of the largest bubble detecting all vapour clusters consisting of empty cells, and selecting the largest among those. However, both methods required an *a priori* setup, starting with the need to identify liquid and vapor molecules with *ad hoc* parameters. Hence, a pre-analysis involving a fine tuning of the parameters for specific thermodynamic conditions is required. This can be avoided by using the *largest spherical cavity* (LSC) method presented here, which is free of adjustable parameters, faster and general, in the sense that it is applicable to liquids featuring very different structures. To test our LSC approach, we will use as benchmark bubble nucleation studies in metastable

a)m.gonzalez12@imperial.ac.uk

water.[22,25] Our approach exploits a subset of the cavity distribution function to compute the Gibbs free-energy of cavity formation in the *NpT* ensemble via the mean first passage time (MFPT) approach.[26] However, the analysis of the total cavity distribution provides a route to obtain the absolute cavity free-energy required to construct the final free-energy barrier. Our work represents the first application of the LSC approach to quantify nucleation free-energy barriers.

One of the key ingredients of the LSC method is the idea of cavity nucleation in a liquid. The concept of "cavity" has been widely used to quantify the structure of fluids. Several decades ago, Reiss *et al.*[27,28] developed the *Scaled Particle Theory* (SPT), which provides a direct link between the statistical distribution of cavities in a fluid and the work (free-energy) needed to create a cavity with a particular radius. This idea has been already exploited to estimate the free-energy of bubble nucleation in simple liquids,[6,19–21,23,24] solute solubility in water,[29,30] or cavitation in simple ionic fluids.[31] In the present manuscript, we use a similar approach to study bubble nucleation in two structurally different liquids, a simple fluid, argon, modelled with the Lennard-Jones potential and liquid water, modelled with the TIP4P/2005 model.[32]

The order parameters employed so far to quantify bubble nucleation free-energies have focused on specific structural characteristics of the liquid of interest, such as, e.g., the coordination number.[22] Given that such properties significantly vary in molecular and simple fluids, it would be very difficult to use the same order parameter to study vapour nucleation in both fluids. To overcome this issue, we propose to use a local order parameter based on the computation of the cavity distribution function, which does not rely on determining structural features specific of the liquid of interest. Our approach relies on the identification of the *largest* cavity that spontaneously nucleates in the system. Once all cavities in the liquid have been identified, we select the largest cavity of the whole set. The computation of the largest cavity over the trajectory can be used to construct the largest cavity distribution function, which is a subset of the total cavity probability distribution function, and that we ultimately use to quantify the bubble nucleation process. Indeed, the nucleation rate and the free-energy barrier can then be calculated from the distribution of the nucleation time of this subset using the MFPT technique.[26] To compute the nucleation free-energy as a function of the total cavity distribution, we make use of the scaled particle theory.

The manuscript is structured as follows. First, we discuss the theoretical background to compute the nucleation rates and the free-energy barriers. Next, we present our results for bubble nucleation in both water and a Lennard-Jones fluid at negative pressures. Finally, we discuss our results and present our main conclusions.

II. METHODS

A. Theoretical background

A liquid equilibrated at a pressure below coexistence becomes metastable and eventually undergoes a phase transition towards a thermodynamically stable vapor phase, via a bubble nucleation process. According to CNT, the nucleation free-energy barrier of the spherical critical bubble is given by

$$\Delta G^* = \frac{16\pi\gamma^3}{3(P_s - P)^2}, \tag{1}$$

where γ is the interfacial free-energy of a liquid-vapour surface at coexistence, P is the pressure at which the nucleation process is being investigated, and P_s is the saturation pressure. The nucleation rate, J, can be written as

$$J = k \exp\left(-\beta \Delta G^*\right), \tag{2}$$

β being $1/k_B T$, where κ_B is the Boltzmann constant, and k is the kinetic prefactor. Following Ref. 33, in a bubble nucleation process, $k = \rho\left(\frac{2\gamma}{\pi m B}\right)$, where ρ is the liquid density, m the atomic or molecular mass and B a factor that takes into account the mechanical equilibrium of the bubble, which is normally set to 1 in cavitation experiments.[33]

When a liquid is stretched at a pressure far from the liquid-vapour binodal and close to the spinodal, the nucleation free-energy barrier is low enough for the vapour phase to nucleate spontaneously in a reasonably short time, which in numerical terms can be of the order of nanoseconds. At these thermodynamic conditions, the mean first passage time[12,34] is a useful tool to compute both nucleation free-energies and rates from the analysis of spontaneously nucleating trajectories. The MFPT approach relies on the evaluation of the *first* time, τ, needed for the chosen order parameter to adopt a specific value. In our bubble nucleation study, we choose as local order parameter the volume of the largest bubble, V, which can be identified with the largest cavity. The average "first times" obtained from the average over many nucleating trajectories gives the "mean" first time, $\tau(V)$, which obeys to the following equation:[12]

$$\tau(V) = \frac{\tau_J}{2}\{1 + erf\left[c(V - V^*)\right]\}, \tag{3}$$

where τ_J is the nucleation time, V^* the volume of the critical bubble, and c a constant proportional to the Zeldovich's factor, $Z = c/\sqrt{\pi}$, which quantifies the curvature of the top of the free-energy barrier. The nucleation rate is expressed as[12,13]

$$J = \frac{1}{\tau_J V_s}, \tag{4}$$

where V_s is the average system's volume, and the nucleation free-energy is given by[26]

$$\beta \Delta G(V) = \ln B(V) - \int \frac{dV'}{B(V')} + D, \tag{5}$$

where D is a reference free-energy that needs to be determined for each system and $B(V)$ is defined as

$$B(V) = -\frac{1}{P(V)}\left(\int_V^{V_m} P(V')dV' - \frac{\tau(V_m) - \tau(V)}{\tau(V)}\right),$$

$P(V)$ being the normalised probability distribution function of finding a bubble of volume V in the metastable state, and V_m the maximum detectable size for the bubble volume, which in this work is set to 4 nm^3 for both liquids (LJ and H_2O). This is a much larger value than the typical volume of the critical nucleus at the thermodynamic conditions under study; thus, our results do not depend on the choice of V_m.

The volume of the largest bubble has been used as a local order parameter in several works and estimated using either grid-based methods[11,16,25] or a Voronoi tessellation approach.[22] Unlike in a recent work by some of us,[25] the volume of the largest bubble is now approximated as that of a spherical cavity with radius, R_{max}, and volume, $V(R_{max}) = 4\pi R_{max}^3/3$, where R_{max} is the *largest cavity radius*, which can be computed using the same algorithms employed to quantify cavity probability distributions in liquids.[31] An advantage of this approach is that the reference free energy, D, can be easily obtained using scaled particle theory concepts.

B. Using the radius of the largest spherical cavity as a local order parameter

Similarly to Ref. 31, our approach relies on the identification of the *largest spherical cavity* spontaneously appearing in the metastable liquid, either in a simple fluid (Lennard-Jones) or in water. Our approach consists of four steps:

Step 1: We build a three dimensional cubic grid that is mapped onto the simulation box. When simulating the isothermal-isobaric (NpT) ensemble, we fix the number of cubic cells in the simulation box; hence, their volume dynamically changes upon rescaling the simulation box. We note that the number of cubic cells in the grid must be sufficiently large to sample the small cavities nucleating in the simulation cell. The final number of boxes employed is a compromise between the CPU time required to locate the cavities and the numerical accuracy. Since our algorithm is not CPU-intensive, we give preference to the accuracy criterion. We find that a cubic cell size with cube side $a = \rho^{-1/3}/3$, $\rho^{-1/3}$ being the average distance between molecules in the fluid, of interest, gives probability distributions that are indistinguishable, within numerical accuracy, from the ones obtained with a larger number of boxes. In this work, we used $L/a = 20$ and 30 cubic cells for water and LJ fluids.

Step 2: For a given cell, the shortest distance between the cell's geometrical centre and the position of every atom (Lennard-Jones) or oxygen atom (water) is computed. This distance corresponds to the distance of the centre of each cell to its nearest atom.

Step 3: We select the cell with the longest distance, R_{max}. For a spherical, that cell would be the one with the largest volume surrounding it and its volume would be given by $V = 4\pi R_{max}^3/3$. Therefore, we propose to use the volume of the largest spherical cavity as the local order parameter. In Fig. 1, we have described our approach in a 2D system. The simulated system consisting of 4 atoms (black circles in Fig. 1) is split into 36 boxes, whose geometric centre is denoted by the red circles. For each cell we calculate the radius of the cavity, which is defined as the distance of the cell geometric centre to any atom in that grid element. From all cavities, we then identify the largest one (see shaded area with blue circle as origin of Fig. 1), whose radius corresponds to the radius of the largest cavity.

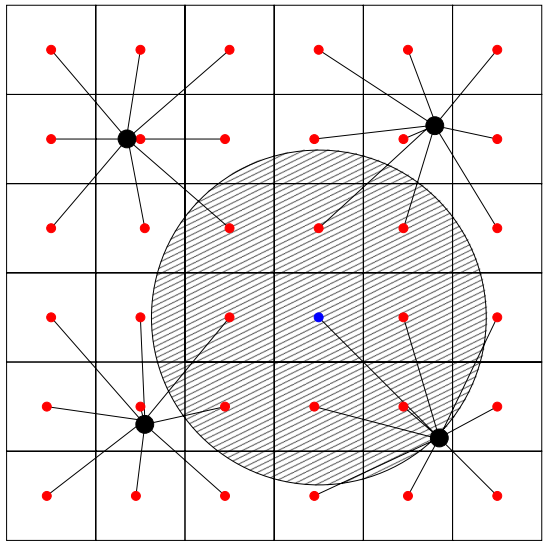

FIG. 1. Illustration of the largest cavity construction in a 2D system. A similar approach was used for the 3D system investigated in this work. The 2D system consists of 4 atoms (black circles) randomly distributed on a plane. The system is then divided in 36 boxes with the same area and whose geometric centres are denoted with the red circles. The black lines indicate the shortest distance of a cell to a given atom. This distance defines the radius of the cavity centered at the cell. The shaded circle represents the cavity with the *largest* radius, which is the *largest cavity* for this specific configuration. We have colored in blue the center of the cell associated to the largest cavity.

Step 4: Next, we construct the cavity probability distribution function $P(V)$. It is then straightforward to compute $\beta\Delta G(V)$ using Eq. (5). To evaluate the reference free-energy, D, appearing in Eq. (5) we compute the *total cavity size probability distribution function*, $P_t(V)$, using *all* cavities spontaneously formed in the system. Note that the main difference between $P_t(V)$ and $P(V)$ is that the latter gives the probability that the largest cavity formed spontaneously in a configuration has volume, V. Hence, $P(V)$ represents a subset of $P_t(V)$. The total cavity size distribution function, P_t, plays a key role in the scaled particle theory[27,28] as it contains information on the reversible work, i.e., the chemical potential difference, $\Delta\mu$, required to create a spherical cavity of radius R in a fluid,

$$\Delta\mu(R) = -k_B T \ln(P_t^{ex}(R)), \tag{6}$$

where the cavity exclusion probability distribution function is given by

$$P_t^{ex}(R) = 1 - \int_0^R P_t(R')dR', \tag{7}$$

$P_t(R)$ being a normalised probability distribution. $P_t(R)$ and $P_t(V)$ play an identical role since V is uniquely defined by its radius R.

It has been shown that the probability distribution function, $P_t(R)$, can be computed analytically for hard spheres of diameter σ whenever $R < \sigma/2$.[27,28] In this case, $P_t(R) = 4\pi R^2\rho$, where ρ is the fluid density. Therefore, Eq. (7) becomes $P_t^{ex}(R) = 1 - 4\pi\rho R^3/3$,

providing an analytical expression for $\Delta\mu$. This analytical relation can also be extended to both the Lennard-Jones and TIP4P/2005 water liquids, even though the condition $R < \sigma/2$ is less strict since these potentials are not discontinuous as in the hard sphere case. Hence, for a given potential, the atomic effective size is determined by the temperature. Higher temperatures allow a deeper penetration in the repulsive region of the potential. The calculation of $\Delta\mu$, where $\Delta\mu \equiv \Delta G$ for large cavity radii requires the integrating the probability distribution function $P_t(R)$. This procedure allows us to estimate the reference free-energy, D, in Eq. (5).

The free-energy barrier is computed using the MFPT technique. This calculation requires the largest cavity probability distribution function $P(V)$ which is defined between (V_0, V_{max}), where $V_0 = 4\pi R_0^3/3$ is the smallest detectable volume and V_{max} is the volume of a post-critical cavity. V_{max} can be arbitrarily chosen, its only requirement being to be larger than the critical volume to allow to evaluate the free-energy at the top of the barrier. The constant D in Eq. (5), corresponding to the work needed to nucleate a cavity with volume V_0, is computed by means of Eq. (6), i.e., $D = -k_B T \ln P_t^{ex}(R_0)$. In our simulations, the sampling of both $P(V)$ and $P_t(V)$ has been performed in the isothermal-isobaric ensemble.

C. Simulation details

We study spontaneous bubble nucleation in two stretched liquids characterised by significantly different thermodynamic and structural properties. We have chosen for our investigation the truncated and shifted LJ (ts-LJ) potential,[35] in order to model the behaviour of a simple liquid, such as argon, and the TIP4P/2005 potential[32] to investigate bubble nucleation in liquid water. Both models have been extensively studied and their liquid-vapour phase diagrams are well characterised.[35–37] These two liquids offer different challenges to the LSC method introduced in this work. First, it has been suggested that the critical bubble in the ts-LJ liquid might not be spherical,[10] although later reports suggest the existence of compact bubbles.[10,11,16] Our order parameter assumes a spherical symmetry for the cavities; hence, the ts-LJ system will be a good benchmark to assess the accuracy of our approximation. Second, water is a liquid that features a lower coordination number than ts-LJ, and also strong orientational correlations. Water will therefore provide a good benchmark to assess whether our local order parameter is robust enough to obtain the nucleation free-energy barrier of complex associating liquids.

We simulate a metastable ts-LJ fluid consisting of 800 particles, in the NpT ensemble at a reduced temperature of $T^* = k_B T/\epsilon = 0.8$ and a reduced pressure of $p^* = p\sigma^3/\epsilon = -0.53$. The Lennard-Jones interactions are truncated and shifted at 4σ, corresponding to a cut-off of 13.62 Å for $\sigma = 3.405$ Å. The simulated state point is relatively close and above the spinodal line ($p^* = -0.6$ at $T^* = 0.8$[17,35]) at thermodynamic conditions where the metastable over-stretched liquid can spontaneously nucleate. The thermodynamic state point has been chosen to compare our results to those reported in Ref. 18.

We have also performed NpT runs of 500 TIP4P/2005 water molecules at metastable conditions, $T = 280$ K and $p = -2250$ bars. The TIP4P/2005 potential was truncated at 9.5 Å and long range pressure corrections were included in the simulations. The long range electrostatic interactions are computed with the particle mesh Ewald method.[38] The geometry of the water molecule is preserved using the SHAKE constraint algorithm.[39] The thermodynamic state point has been chosen above the spinodal line to compare with the results reported in the previous works.[22,40]

In both Lennard-Jones and water liquids, we simulate and analyse 200 independent spontaneously nucleating trajectories starting from configurations initiated with random velocities extracted from a Maxwell-Boltzmann distribution. In both systems, we use the leapfrog algorithm with a timestep of 1 fs, to integrate the equations of motion along with the velocity rescaling thermostat[41] (with relaxation time $\tau_T = 1$ ps) and the Parrinello-Rahman barostat[42] (with relaxation time $\tau_p = 2$ ps) to generate the NpT ensemble trajectories. All simulations are performed with the molecular dynamics package GROMACS v 4.5.[43]

III. RESULTS AND DISCUSSION

We start our discussion by analysing the ability of LSC order parameter to identify the vapour nucleation process in both liquids, ts-LJ and TIP4P/2005 water. In Figure 2, we represent the volume of the largest cavity (computed as $4\pi R_{max}^3/3$) as a function of time for two independent nucleating trajectories of both water and ts-LJ liquid. The largest cavity undergoes large volume fluctuations until it reaches the transition to the vapour phase, which is characterised by a sharp increase in the cavity volume. Our LSC order parameter captures well the volume fluctuations of the background cavities and identifies the onset of nucleation, where the cavity radius abruptly grows. The time at which the transition occurs

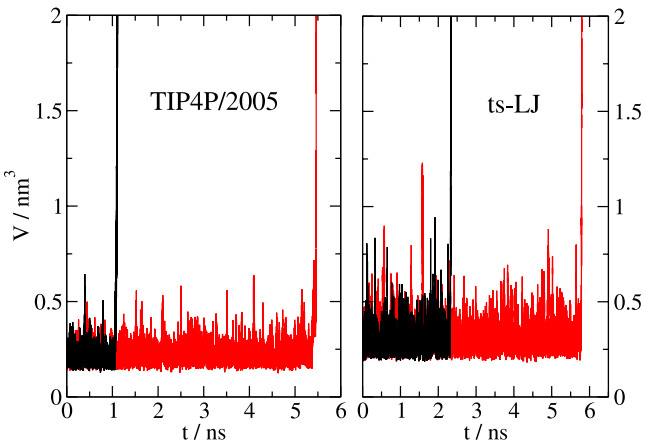

FIG. 2. Evolution of the volume of the largest spherical cavity for two independent trajectories (in black and red) for TIP4P/2005 water (left panel) and the ts-LJ (right panel). Notice that the scale is the same for the two systems.

defines the nucleation time for that specific trajectory and, as expected for a stochastic process, this time varies significantly from one configuration to another. However, we have observed that at the chosen thermodynamic states the nucleation times of all simulated trajectories are of the order of a few ns, which enables the sampling of many trajectories in a reasonable computational time.

Comparing the fluctuations of both metastable liquids (see Figure 2), we observe that water tends to generate cavities with smaller volumes than the Lennard-Jones. This, together with the different thermodynamic conditions of water and the Lennard-Jones liquid, $(T_c^*/T^*)_{ts-LJ} \approx 1.6$ vs. $(T_c/T)_{water} \approx 2.3$ (where $T_c^* = 1.246$ for ts-LJ[35] and $T_c = 640$ K for water model[36]), explains the differences observed across both liquids, LJ being closer to its critical point.[22,29]

In order to confirm that our assumption of modelling a bubble as a spherical cavity is acceptable, we show in Figure 3

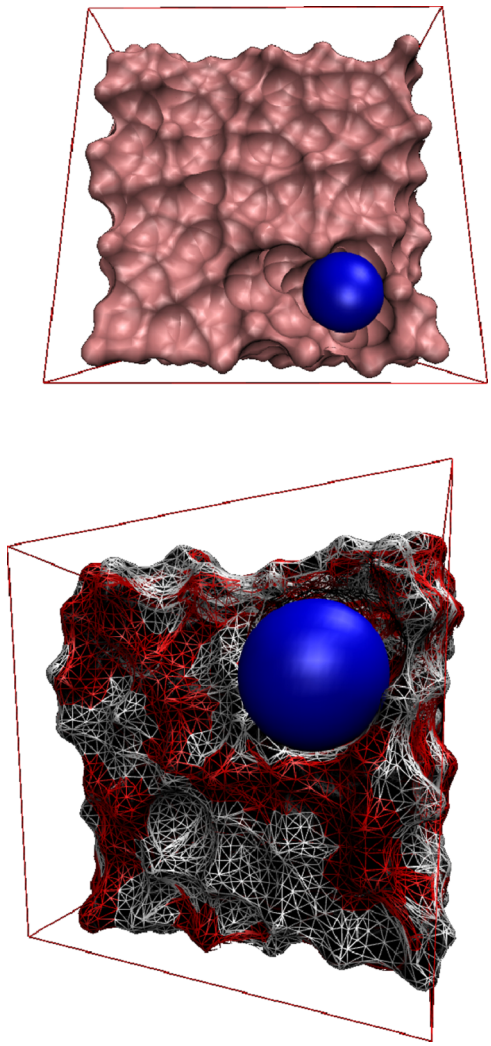

FIG. 3. (Top) Snapshot of the metastable ts-LJ liquid showing the largest precritical bubble. The pale pink surface around each ts-LJ atoms has been rendered using Visual Molecular Dynamics (VMD).[44] The blue sphere represents the largest cavity detected by the LSC method for this configuration. (Bottom) Snapshot of the metastable water configuration showing the largest precritical bubble. The surface around the water molecules has been rendered using VMD.[44] The red and white bonds represents oxygen and hydrogen atoms, respectively. In both panels, the red lines represent the simulation box.

a snapshot featuring typical precritical cavities in metastable water and ts-LJ liquids. By construction, the LSC method approximates the volume of the cavity as that of the largest sphere that can be accommodated within the bubble. From a visual inspection, we can argue that the spherical geometry nicely adjusts to the shape of the bubble in both systems. Our results seem to support the predictions of Ref. 16 (in the case of Lennard-Jones) and Refs. 22 and 25 (in the case of water).

Figure 4 shows the largest cavity probability distribution, $P(V)$. In agreement with our previous discussion, the most probable cavity volume—which corresponds to the maximum of $P(V)$—is larger for the ts-LJ ($\approx$0.28 nm^3) than for water ($\approx$0.19 nm^3). Having computed $P(V)$, we can now evaluate the nucleation free-energy via the MFPT method (see Eq. (5)) as discussed in Secs. II A and II B.

In order to compute the free-energy barrier with the MFPT method, we need to evaluate the nucleation time, τ, from the nucleating trajectories. In Figure 5, we represent the average time required for a cavity of volume V to appear for the first time in a trajectory, $\tau(V)$, as a function of its volume for both water and Lennard-Jones liquids. The results for water were obtained from the analysis of the trajectories generated in Ref. 22. We recall that in that work the largest bubble was identified using the Voronoi tessellation method. The nucleation time, defined as the time needed to reach a plateau in $\tau(V)$, shows excellent agreement with the previous estimates based on the Voronoi construction.[22] Notice that the average time, $\tau(V)$, can be evaluated with the LSC method at a fraction of the computational costs needed to generate the Voronoi tessellation. The main difference between the Voronoi and the LSC approaches lies in the estimation of the volume of the nucleating bubble. The Voronoi construction maps the growing bubble onto a polyhedron, hence accounting for the bubble's irregularities while the LSC method approximates the bubble's volume to that of the largest inscribed sphere. The difference between the Voronoi and LSC volume is also related to the approach used in Ref. 22 where the volumes where adjusted to remove the effect of interfacial molecules.

The inflection point in $\tau(V)$ defines the time needed to reach the critical volume, V^*. In Fig. 5, we observe that this

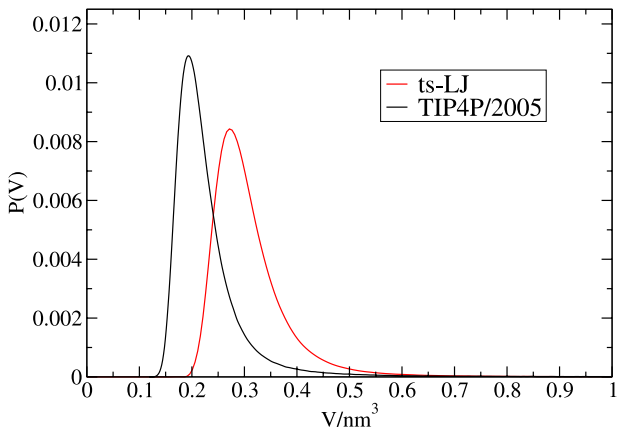

FIG. 4. Normalised largest cavity probability distribution as a function of the cavity volume V. The black line corresponds to the TIP4P/2005 water and the red to the ts-LJ liquid.

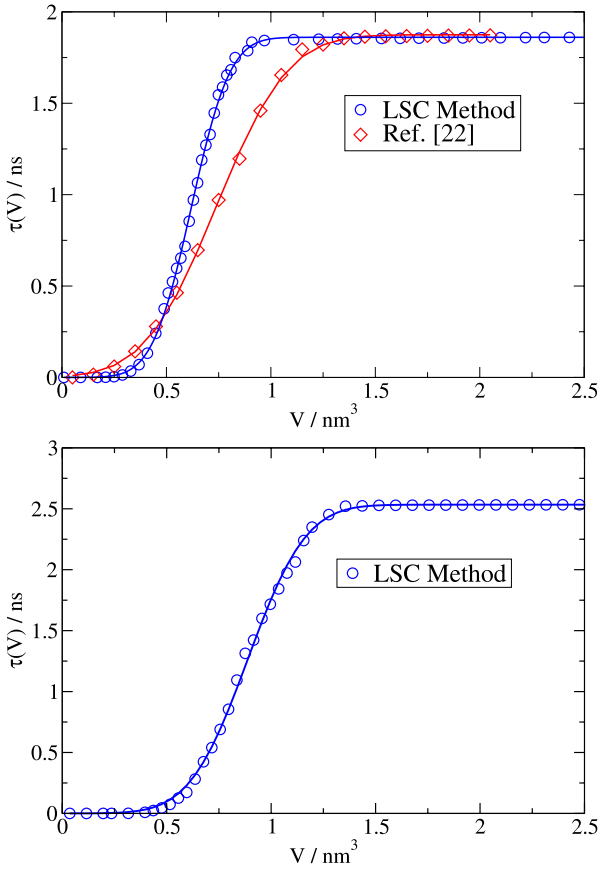

FIG. 5. (Top) MFPT for TIP4P/2005 water obtained with the LSC method (blue circles) and with Voronoi construction[22] (red diamonds). Both data sets are at the same thermodynamic conditions, $T = 280$ K and $p = -2250$ bars, and were obtained from the analysis of the trajectories generated in Ref. 22. (Bottom) MFPT distribution for the ts-LJ liquid at $T^* = 0.8$ and $p^* = -0.53$. In both panels, the solid lines represent the fit of Eq. (3).

time is fairly independent on the method employed, being 0.94 ns for the Voronoi tessellation method and 0.93 ns for LSC. We find that the critical volume estimated via the Voronoi tessellation method is ∼15% larger than that predicted with the LSC method. However, these volume differences have a small impact on the estimated critical radii. Given the cubic dependence of the volume with the radius, the critical radius is 0.56 nm in the Voronoi case (assuming a spherical geometry) and 0.54 nm using the LSC method. Following the same approach, we have estimated the volume (radius) of the critical nucleus in the Lennard-Jones metastable liquid. Previous works on superheated LJ liquids provide a good reference to assess the accuracy of our calculations. Shen and Debenedetti[45] evaluated the critical radius for different values of $\Delta\mu/\Delta\mu_{spin}$, where $\Delta\mu = \mu - \mu_{sat}$ and $\Delta\mu_{spin} = \mu_{spin} - \mu_{sat}$, μ being the chemical potential at the thermodynamic state of interest, and the subscripts referring to the saturation and the spinodal line. One advantage of using $\Delta\mu/\Delta\mu_{spin}$ to compare different simulation results is that this ratio is independent of the cut-off employed to truncate the pair potential.[18,45] We note that the location of the coexistence and the spinodal lines depends on the truncation radius. The chemical potentials needed to compare our results with those reported by different authors were obtained from the equation of state of Johnson *et al.*[35] At the chosen thermodynamic conditions, we obtain $\Delta\mu/\Delta\mu_{spin} = 0.87$ which corresponds, according to Fig. 4 in Ref. 18, to a critical radius of 0.57 nm. This result is in very good agreement with our LSC prediction of 0.59 nm for the same $\Delta\mu/\Delta\mu_{spin}$ ratio.

Next, we computed the nucleation rate, J, by means of Eq. (4), assuming $V_s = 17.1$ nm^3 for water and 45.1 nm^3 for the ts-LJ liquid (numerical results are reported in Table I). The rate for water is $J = 3.15 \times 10^{28}$ cm^{-3} s^{-1}, in very good agreement with the one reported in Ref. 22 at the same thermodynamic state. As stated in Ref. 22, the CNT significantly underestimates the nucleation rate. Indeed, the values obtained in that work are about 10 orders of magnitude larger than the CNT prediction, $J_{CNT} = 1.7 \times 10^{-10}$ nm^{-3} ns^{-1} vs. $J_{LSC} = 3.15$ nm^{-3} ns^{-1}. Notice that the CNT value for J is extremely sensitive to the liquid-vapour interfacial energy γ, as it depends exponentially on ΔG^*, which in turn features a cubic dependence on γ (see Eq. (1)). The surface tension is often assumed to be the surface tension of a planar liquid-vapour interface at coexistence. However, it has been shown in numerical studies that curvature effects influence the interfacial tension at nanometer length-scales,[46,47] which would also affect the characteristic size of the critical radius.

When computing the nucleation rate, we also estimated the Zeldovich factor. Our predictions for water are in line with the previous estimates (see Table I). The Voronoi approach predicts a slightly lower value, which indicates that the curvature of the free-energy barrier obtained via the Voronoi construction is smaller than in the LSC case.

Finally, we compute the nucleation free-energy barriers for both liquids. These free-energies were obtained from the LSC probability cavity distribution function and the MFPT analysis (Eqs. (5)[13,26] and (6)[31]). As already stated in Sec. II, in order to estimate the reference free-energy, D, appearing in Eq. (5) we use the *total* cavity probability distribution P_t. In Figure 6 (top panel), we show P_t for TIP4P/2005 water, sampled in both *NpT* and *NVT* ensembles, using *all* volumes present in the system *before* cavitation takes place. At the same time, we compute $\Delta\mu$ for both *NVT* and *NpT* ensemble, as shown in Fig. 6 (bottom panel), that defines the constant D. It is clear that the ensemble has a large impact on the probability distribution, P_t, particularly in the nucleation of large cavities, which is more likely in the *NpT* case, where the volume of the simulation box is allowed to fluctuate, hence leading to a lower chemical potential. For the same cavity volume, constraining the box volume results in an overestimation of

TABLE I. Nucleation time (τ_J/ns), Zeldovich factor (Z/nm^{-3}), critical volume (V^*/nm^3), nucleation rate ($J/10^{28}$ cm^{-3} s^{-1}), and free-energy barrier (ΔG^*) for TIP4P/2005 water at 280 K and −2250 bars and ts-LJ at $T^* = 0.8$, $p^* = -0.53$. LSC corresponds to the results obtained in this work while Voronoi and DFT represent those reported in Refs. 22 and 18, respectively.

Liquid	Method	τ_J	Z	V^*	J	$\beta\Delta G^*$
Water	LSC	1.86	2.73	0.63	3.15	11
Water	Voronoi[22]	1.87	1.48	0.74	3.10	10
ts-LJ	LSC	2.62	1.84	0.87	8.46	11
ts-LJ	DFT[18]	...	...	0.36	...	10

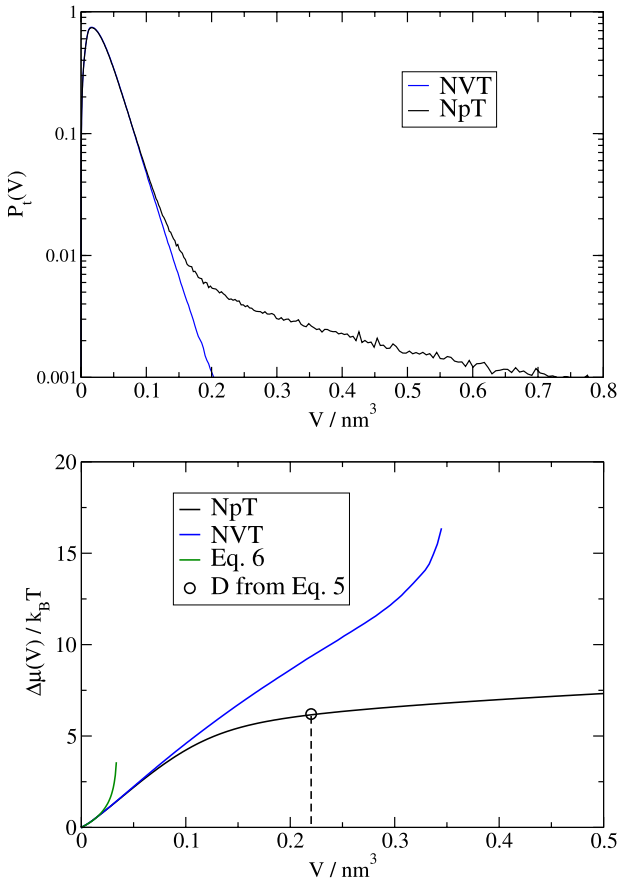

FIG. 6. (Top) Normalised cavity probability distribution function P_t sampled in both *NpT* (black) and *NVT* (blue) ensembles for TIP4P/2005 water. (Bottom) $\Delta\mu$ for the ensembles computed in the top panel. The dark green lines shows the analytical solution obtained from Eq. (6). The empty circle represents our estimate of the reference free-energy D (see Eq. (5)), about 6 k_BT at $V_0 = 0.23$ nm^3.

$\Delta\mu$ of about 2 k_BT. This has to be taken into account when choosing the ensemble to compute the free-energy reference D. Therefore, in order to compute D, we employ the *NpT* ensemble to be consistent with the *NpT* computations of the free-energy barrier. We also show in Figure 6 the analytical predictions of $\Delta\mu$ (see discussion in Step 4, Sec. II B). The small volume region is well reproduced by the analytical formula, $P_t^{ex}(R) = 1 - 4\pi\rho R^3/3$. However, deviations between this equation and the simulation results are observed for larger volumes $V > 0.02$ nm^3, which correspond to radii > 0.16 nm. This threshold radius corresponds to a half of the diameter of the Lennard Jones atoms or about half of the diameter of the Lennard-Jones site (oxygen) in the TIP4P/2005 water.

For wate,r we find $D = 6\ k_BT$ and $V_0 = 0.23$ nm^3 whereas for the ts-LJ liquid $D = 5.5\ k_BT$ and $V_0 = 0.28$ nm^3. Having determined the constant D for both TIP4P/2005 and ts-LJ liquid, we estimate the corresponding nucleation free-energy barriers (Figure 7). For both models, the nucleation free-energy features a maximum ($\beta\Delta G^*$) at the critical cavity's volume. We report in Table I the numerical results of the free-energy barrier and compare them with the previous studies. The free-energy barriers for both water and ts-LJ are within $\sim 1\ k_BT$ of those estimated in Refs. 22 (water) and 18 (ts-LJ).

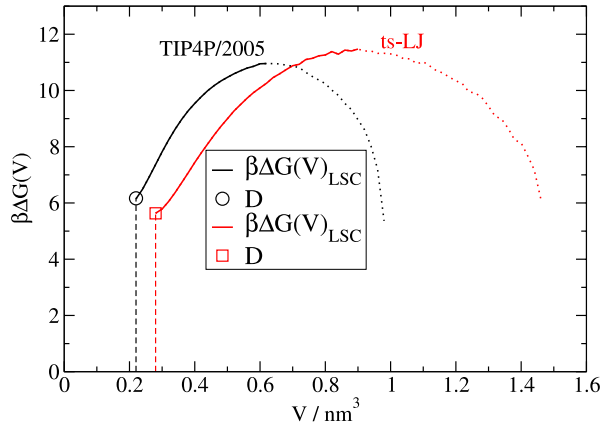

FIG. 7. Nucleation free-energy barrier as a function of the cavity largest spherical volume estimated using the LSC method for the TIP4P/2005 (solid black line) and the ts-LJ liquids (solid red line). The dotted lines represent the free-energy beyond the top of the barrier whereas the empty symbols represent our D values.

These differences are within the expected uncertainty associated to state of the art free-energy methods.

IV. CONCLUSIONS

In this work, we have introduced a local order parameter to investigate bubble nucleation in two metastable liquids at negative pressure, TIP4P/2005 water and a Lennard-Jones fluid, whose translational and orientational structures are significantly different: the Lennard-Jones fluid is dominated by packing constraints, whereas hydrogen bonds impose a low coordination structure and a high degree of orientational ordering in water. Our order parameter is based on the identification of the *largest spherical cavity* that nucleates spontaneously in the over-stretched metastable liquid. The implementation of such order parameter only requires the calculation of a radial distance, making redundant the use of additional geometric criteria, such as monitoring local coordination numbers, or more intensive computational approaches to map the bubbles' volume into polyhedra. By computing the volume of the largest spherical cavity of several spontaneously nucleating trajectories, one can use the mean first passage time technique to efficiently estimate nucleation properties.

The critical bubble radii, free-energy barriers, and nucleation rates of water and the Lennard-Jones liquid are in very good agreement with the previous estimates based on either Voronoi constructions or grid-based methods. The free-energy barriers obtained here are within $\sim 1 k_BT$ of the values reported in the literature using different approaches, such as umbrella sampling.

The LSC method offers some advantages over the previous approaches. First of all, it is not system-dependent and may be used in a wide range of liquids, featuring different structural properties. States where the density is low, e.g., near the critical point and superheated liquids may pose some challenges to our current implementation of the LSC method. In these cases, the cavity probability distribution might not be so well defined, making more difficult the localization of the nucleating bubble. In these high temperature states, it is

also expected that the vapour density is not negligible and the cavity approximation to describe the bubble may become less accurate. These specific situations have been considered in the previous studies using different methods (see, e.g., Ref. 22), which rely on the use of clustering criteria to identify the largest vapour bubble.[16,23,24]

Despite these shortcoming, which are restricted to the high temperature region of the phase diagram, the LSC method provides clear advantages over the previous approaches: it is easy to implement and computationally efficient. Our analysis indicates that moderate grid sizes are enough to obtain the cavity probability distribution function, making the method computationally inexpensive. However, the main strength of the method is its generality, as it circumvents the need to define clustering approaches, or to define specific criteria that require previous knowledge of the structural properties of the fluid of interest. Given its versatility and numerical efficiency, the LSC method can be extended to investigate heterogeneous vapour nucleation involving complex substrates. Work in this direction is in progress.

ACKNOWLEDGMENTS

We thank the Imperial College High Performance Service for providing computational resources. M.A.G. acknowledges both the "Thomas Young Centre" for the award of a Junior research Fellowship and the "Pan-European Research Infrastructure on High Performance Computing (HPC-EUROPA2)" for the award of a travelling Fellowship. F.B. acknowledges the EPSRC (EP/J003859/1) for the award of a Leadership Fellowship. C.V. acknowledges Spanish Grant No. JCI-2010-06602 and EU Grant No. 322326-COSAAC-FP7-PEOPLE-CIG-2012. M.A.G., C.V., and J.L.F.A. acknowledge Spanish Grant No. FIS2013-43209-P.

APPENDIX: COMPARISON BETWEEN LSC AND VORONOI METHODS AND DEPENDENCE OF THE PROBABILITY CAVITY DISTRIBUTION FUNCTION WITH THE NUMBER OF CUBIC CELLS

We have compared the volumes obtained with the LSC and Voronoi methods by applying the algorithms to the same trajectory. We chose one trajectory used to obtain the Voronoi data reported in a previous work.[22] The trajectory corresponds to a system consisting of 500 water molecules at 280 K and −2250 bars. We show in Fig. 8 the volume of the largest cavity compared to that corresponding to the modified Voronoi polyhedra volume obtained as discussed in Ref. 22, whereby the critical bubble volume is given by the Voronoi construction subtracting the volume associated to the interfacial water molecules. These two definitions naturally result in slightly different volumes for the bubble, but it is clear from inspection of our Figure 8, that both identify the same cavities. This can be easily seen by comparing the fluctuations of the LSC and Voronoi methods which show a perfect correlation.

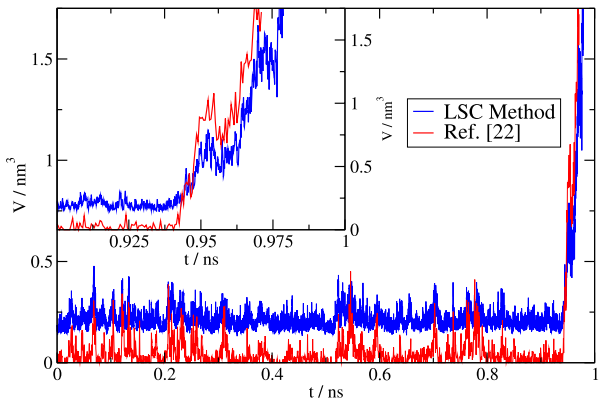

FIG. 8. Evolution of the volume of the largest spherical cavity and the volume obtained from the Voronoi construction reported in Ref. 22. The results corresponds to a spontaneous nucleation event in TIP4P/2005 water at negative pressures.

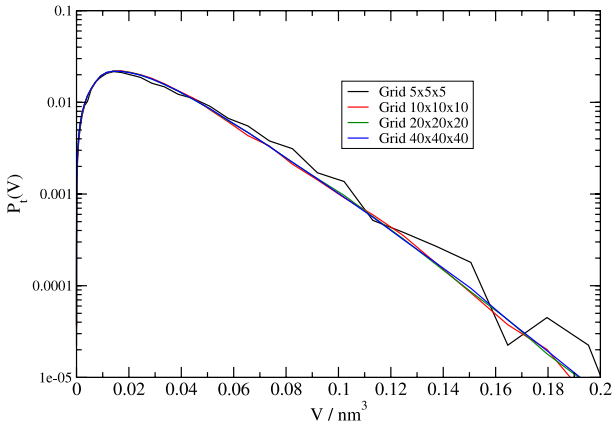

FIG. 9. Total cavity distribution function averaged over 100 configurations for TIP4P/2004 water as a function of the number of cubic cells employed to partition the simulation box. The results correspond to a metastable liquid at 280 K and −2250 bars.

The inset of Fig. 8 shows a fragment of the trajectory around the cavitation event. The critical volume of the bubble obtained with the Voronoi tessellation is found to be slightly larger than the one defined by the LSC approach. This result is representative of the general behavior we find for many independent trajectories and explains the slightly larger volume found in the Voronoi approach as compared with the LSC one (see Table I).

We show in Fig. 9 the total cavity distribution function averaged over 100 configurations for TIP4P/2004 water as a function of the number of grid cells. The thermodynamic conditions are the same as those discussed above and the configuration does not contain a critical cavity. It is evident that the distribution is independent of the grid size for 20^3 cells or more.

[1]M. Volmer and A. Weber, Z. Phys. Chem., Stoechiom. Verwandtschaftsl. **119**, 277 (1926).
[2]P. G. Debenedetti, *Metastable Liquids* (Princeton University Press, Princeton, New Jersey, 1996).
[3]C. F. Delale, J. Hruby, and F. Marsik, J. Chem. Phys. **118**, 792 (2003).
[4]X. C. Zeng and D. W. Oxtoby, J. Chem. Phys. **94**, 4472 (1991).
[5]V. Talanquer and D. Oxtoby, J. Chem. Phys. **102**, 2156 (1995).
[6]M. J. Uline and D. S. Corti, Phys. Rev. Lett. **99**, 076102 (2007).
[7]R. Y. Yang, R. P. Zou, and A. B. Yu, Phys. Rev. E **65**, 041302 (2002).
[8]G. Torrie and J. Valleau, Chem. Phys. Lett. **28**, 578 (1974).
[9]S. Auer and D. Frenkel, Nature **409**, 1020 (2001).
[10]V. K. Shen and P. G. Debenedetti, J. Chem. Phys. **111**, 3581 (1999).
[11]S. L. Meadley and F. A. Escobedo, J. Chem. Phys. **137**, 074109 (2012).
[12]J. Wedekind, R. Strey, and D. Reguera, J. Chem. Phys. **126**, 134103 (2007).
[13]J. Wedekind, G. Chkonia, J. Woelk, R. Strey, and D. Reguera, J. Chem. Phys. **131**, 114506 (2009).

[14]K. S. Suslick, Science **247**, 1439 (1990).
[15]Y. Chen and J. Israelachvili, Science **252**, 1157 (1991).
[16]Z.-J. Wang, C. Valeriani, and D. Frenkel, J. Phys. Chem. B **113**, 3776 (2009).
[17]S. Punnathanam and D. S. Corti, Ind. Eng. Chem. Res. **41**, 1113 (2002).
[18]S. Punnathanam and D. S. Corti, J. Chem. Phys. **119**, 10224 (2003).
[19]S. Punnathanam and D. S. Corti, J. Chem. Phys. **120**, 11658 (2004).
[20]M. J. Uline and D. S. Corti, J. Chem. Phys. **129**, 234507 (2008).
[21]K. Torabi and D. S. Corti, J. Chem. Phys. **133**, 134505 (2010).
[22]J. L. F. Abascal, M. A. Gonzalez, J. L. Aragones, and C. Valeriani, J. Chem. Phys. **138**, 084508 (2013).
[23]K. Torabi and D. S. Corti, J. Phys. Chem. B **117**, 12479 (2013).
[24]K. Torabi and D. S. Corti, J. Phys. Chem. B **117**, 12491 (2013).
[25]M. A. Gonzalez, G. Menzl, J. L. Aragones, P. Geiger, F. Caupin, J. L. Abascal, C. Dellago, and C. Valeriani, J. Chem. Phys. **141**, 18C511 (2014).
[26]J. Wedekind and D. Reguera, J. Phys. Chem. B **112**, 11060 (2008).
[27]H. Reiss, H. Frisch, and J. Lebowitz, J. Chem. Phys. **31**, 369 (1959).
[28]H. Reiss, H. Frisch, E. Helfand, and J. Lebowitz, J. Chem. Phys. **32**, 119 (1960).
[29]A. Pohorille and L. Pratt, J. Am. Chem. Soc. **112**, 5066 (1990).
[30]L. Pratt and A. Pohorille, Proc. Natl. Acad. Sci. U. S. A. **89**, 2995 (1992).
[31]F. Bresme and J. Alejandre, J. Chem. Phys. **118**, 4134 (2003).
[32]J. L. F. Abascal and C. Vega, J. Chem. Phys. **123**, 234505 (2005).
[33]M. Blander and J. L. Katz, AIChE J. **21**, 833 (1975).
[34]G. Chkonia, J. Woelk, R. Strey, J. Wedekind, and D. Reguera, J. Chem. Phys. **130**, 064505 (2009).
[35]J. K. Johnson, J. A. Zollweg, and K. E. Gubbins, Mol. Phys. **78**, 591 (1993).
[36]C. Vega, J. L. F. Abascal, and I. Nezbeda, J. Chem. Phys. **125**, 034503 (2006).
[37]M. M. Conde, M. A. Gonzalez, J. L. F. Abascal, and C. Vega, J. Chem. Phys. **139**, 154505 (2013).
[38]U. Essmann, L. Perera, M. L. Berkowitz, T. Darden, H. Lee, and L. G. Pedersen, J. Chem. Phys. **103**, 8577 (1995).
[39]J. P. Ryckaert, G. Ciccotti, and H. J. C. Berendsen, J. Comput. Phys. **23**, 327 (1977).
[40]M. A. Gonzalez, Master's thesis, Facultad de Ciencias Quimicas, Madrid, 2011.
[41]G. Bussi, D. Donadio, and M. Parrinello, J. Chem. Phys. **126**, 014101 (2007).
[42]M. Parrinello and A. Rahman, J. Appl. Phys. **52**, 7182 (1981).
[43]B. Hess, C. Kutzner, D. van der Spoel, and E. Lindahl, J. Chem. Theory Comput. **4**, 435 (2008).
[44]W. Humphrey, A. Dalke, and K. Schulten, J. Mol. Graphics **14**, 33 (1996).
[45]V. K. Shen and P. G. Debenedetti, J. Chem. Phys. **114**, 4149 (2001).
[46]F. Bresme and N. Quirke, J. Chem. Phys. **110**, 3536 (1999).
[47]F. Bresme, H. Lehle, and M. Oettel, J. Chem. Phys. **130**, 214711 (2009).